Accepted Article

Polymers of Intrinsic Microporosity (PIMs) in Triphasic Electrochemistry: Perspectives

Prof. Frank Marken [1]*, Dr. Elena Madrid [1], Yuanzhu Zhao [1],
Dr. Mariolino Carta [2], and Prof. Neil B. McKeown [3]

[1] *Department of Chemistry, University of Bath, Bath BA2 7AY, UK*

[2] *Department of Chemistry, Swansea University, College of Science, Grove Building, Singleton Park, Swansea SA2 8PP, UK*

[3] *EAstChem School of Chemistry, University of Edinburgh, Joseph Black Building, David Brewster Rd., Edinburgh, Scotland EH9 3FJ, UK*

To be submitted as review to ChemElectroChem

Proofs to F. Maken (F.marken@bath.ac.uk)

Abstract

Polymers of intrinsic microporosity (PIMs) as molecularly rigid polymers have emerged as a new class of gas permeable glassy materials. They offer excellent processability and a range of potential applications also in electrochemical processes. Particularly interesting is the ability of some PIM films to remain gas-permeable/binding even in the presence of (aqueous) liquid electrolyte to give triphasic interfacial reactivity. Gaseous reagents or products (such as hydrogen or oxygen) are bound probably into hydrophobic regions in the wet PIM film to avoid macroscopic bubble formation and to enhance both the surface reactivity and the apparent activity of the gas solute close to the electrode/catalyst surface. The photo-electrochemical formation of hydrogen gas close to a platinum electrode is enhanced by PIM-1, which is presented as an example of energy harvesting via molecular H_2 "energy carrier" transport.

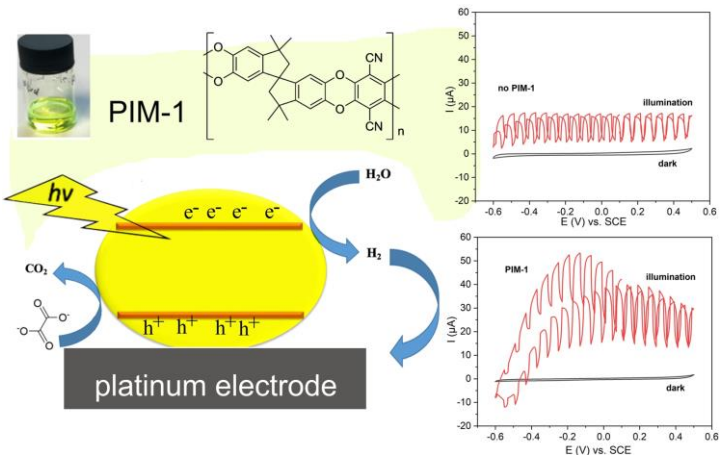

Graphical Abstract:

ToC: As a novel class of processeable glassy porous polymer materials, PIMs offer diversity in terms of molecular structure and porosity, as well as opportunities in terms of multi-phase interactions in the vicinity of electrode/catalyst surfaces. Exploratory research reviewed here shows that the presence of a thin film of porous polymer can significantly affect electrochemical and membrane processes. The molecular rigidity of the polymer allows the environment of electrodes/catalysts to be modified in particular for gas evolving and consuming reactions.

Keywords: Electrochemistry; electrocatalysis; modified electrodes; triphasic catalysis; ion conductivity; ionic diodes; gas diffusion electrodes

Content

1. Introduction to Triphasic Electrocatalysis

Electrochemical reactions often are associated with phase formation, multi-phase systems, or phase boundaries: gas evolution,[1] gas consumption,[2] liquid-liquid based interfaces and/or droplets with a triple phase boundary reaction zone,[3,4] nucleation of bubbles or solid particles,[5,6] or collisions of solid particles with the electrode surface.[7] The interaction and reactivity of particles, droplets, or bubbles changes with distance from the electrode surface and with interface design. The case for gas bubble to surface interaction is illustrated schematically in Figure 1. The concentration of the gaseous species in solution is denoted $c_{solution}$.

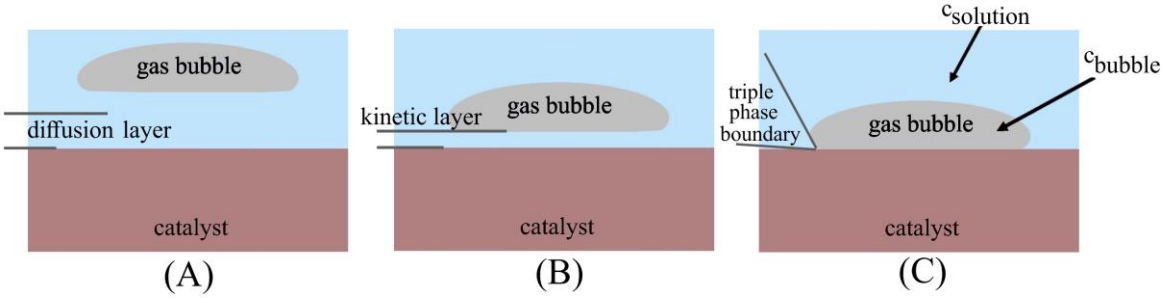

Figure 1. Gas evolution: schematic illustration of gas|liquid|solid interactions for (A) dissolved gas and transport based on a diffusion boundary layer, (B) a bubble approaching the surface to give a kinetic boundary layer, and (C) a bubble interacting with the surface resulting in a triple phase boundary.

The flux of a gaseous solute from the bubble surface to the solid electrode surface (or in opposite direction) is dependent on the concentration $c_{solution}$ and the distance across which the transport occurs (assuming Nernstian transport with flux = D dc/dx). If this distance is outside of that for the diffusion layer (Figure 1A), then the process becomes distance independent and limited by $c_{solution}$. However, for a distance within the diffusion layer (Figure 1B), the rate of transport is enhanced and the "apparent solution concentration" appears increased (up to the transport/kinetic limit as the distance decreases). Therefore, bringing gas bubbles closer to the reactive surface should enhance reaction rates. In particular, very small bubbles with high internal pressure should be beneficial for enhanced reaction rates. However, for a gas bubble firmly attached to the solid surface, a substantial part of the reactive surface is blocked/passivated and only the triple phase boundary zone (Figure 1C) remains active for electrochemical reactions. Based on this reasoning, processes would generally benefit from gaseous reactants in very small nanobubbles being present very close to the surface without any direct attachment to the surface or blocking. However, managing multi-phase systems close to an electrode surface can be complex, in particular when considering the inter-dependency of mass transport and phase separation.

The design of liquid | solid | gas interfaces can be employed to improve reactivity. Recently, Cui and coworkers developed a highly efficient electrocatalytic CO_2 reduction process based on an extended three-phase boundary interface engineered into an assembly of a gold electrode and a polymeric film of commercial nano-poly-ethylene.[8] The process was compared to the natural phenomenon of enhanced gas exchange in lungs, where effective exchange of oxygen and CO_2 are linked to the presence of alveoli creating an extended triple phase boundary region. Therefore, interfacial design for triphasic systems offers real benefits in reactivity. A very similar concept of a "breathing catalyst" with high triple phase boundary region was realised by Cui *et al*. also for the oxygen reduction and evolution reactions.[9] Other types of related gas diffusion electrodes for CO_2 reduction have been developed for example by Wessling and coworkers.[10]

The level of multi-phase complexity in both gas evolution and gas consumption reactions can be even higher when bubble nucleation and transport are involved. For example, when a gas bubble adheres to a catalyst surface, this causes blocking. As a result, the catalytic reaction

would cease or diminish in rate and effects would be observed as apparently lower rate constants and/or higher overpotentials. A possible method to avoid catalyst blocking can be based on nano-structured catalysts, for example based on highly microporous frameworks and/or hierarchical architectures that prevent gas bubbles from directly interacting with the internal catalyst surface (see Figure 2B). There are many recent examples for gas evolving electrodes with hierachical nano-structures[11] to make processes highly effective. Studies at individual nano-electrodes (by White and coworkers[12]) have provided better insight into the conditions during nano-bubble nucleation with critical bubble sizes for example for hydrogen on platinum of below 10 nm. The energy required for the formation/nucleation of such small nano-bubbles within the nano-structure can be very high (for hydrophilic surfaces), which may lead to supersaturation and bubble nucleation only on the outside to maintain a high catalyst reactivity (Figure 2B).

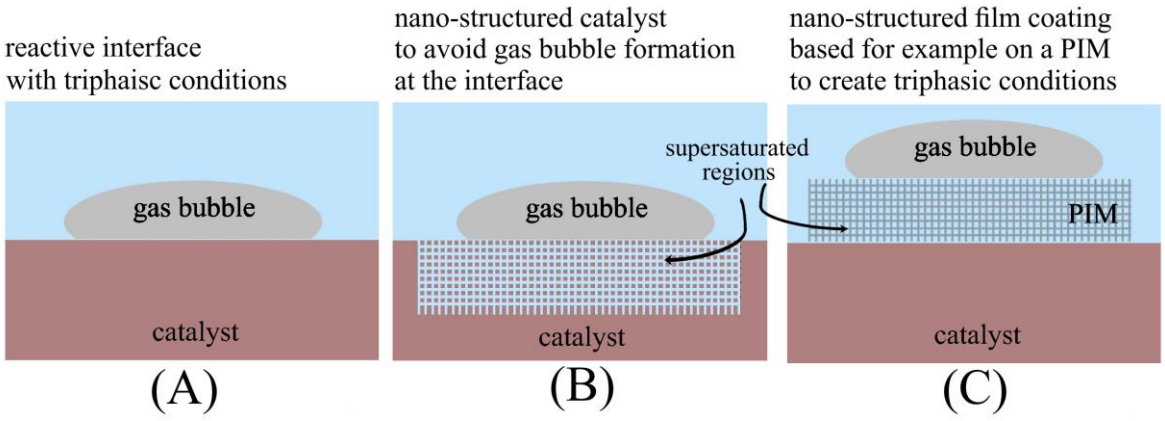

Figure 2. Enhanced gas reactivity at nano-strutured interfaces: (A) at a featureless interface, (B) at a nano-structured catalysts/electrode surface, and (C) with a nano-structured "gas managmenet layer" applied to avoid bubble blocking.

An alternative approach to avoiding interfacial bubble formation could be based on applying a nano- or microporous structure on the outside of the catalyst in the form of a "gas management layer" (Figure 2C). The conditions for a material to be beneficial as gas management layer are (i) good processability to readily deposit/cast films from a solution, (ii) a non-blocking interaction with the catalyst surface, (iii) good uniformity and minimal porosity aging, (iv) ability to allow both gaseous and liquid phase to permeate simultaneously under triphasic conditions, (v) binding of the gaseous species, and (vi) good chemical

robustness. Many of these points can be addressed with a new class of molecularly rigid materials: polymers of intrinsic microporosity or "PIMs".[13]

Figure 2 summarises the cases of (A) a gas bubble blocking the reactive surface, (B) a nano-structured reactive surface to bypass the interfacial bubble, and (C) the case of a "gas management layer" that allows transport and increased activity of the gaseous species. The nucleation of bubbles within microporous structures or at the surface can be understood (at least in first approximation) based on classical Young-Laplace theory,[14] which suggests that bubble nucleation is energetically difficult at the nanoscale (for hydrophilic surfaces) leading to supersaturation. Note also distinct effects of the nature of the gas solute on nucleation of bubbles due to changes in interfacial tension.[15] Hydrophobic regions (e.g. within some of the PIM materials) could provide regions for binding and transport of gaseous solutes at the nanoscale. This will be further discussed below.

2. Introduction to Polymers of Intrinsic Microporosity

A wide range of novel mesoporous and microporous materials have emerged such as zeolites,[16,17] metal organic frameworks,[18,19] and covalent organic frameworks[20] with the an open network of micropores (ranging typically from 0.5 nm to 5 nm or higher). Many polymers are known to be microporous and gas permeable and particularly glassy polymers with high excess free volume are of interest[21] for example in gas separation.[22] These can be cross-linked materials[23] (which are difficult to process), but also moleculary rigid processable materials such as polymers of intrinsic microporosity or PIMs.[24,25] Figure 3 shows a selection of structural motifs in PIMs. These materials are formed via condensation reactions and generally require sufficiently high molecular weights (e.g. 50 to 100 kDa depending on the molecular structure) to avoid brittleness. The highly rigid molecular backbone imparts the unusual materials properties by limiting inter-molecular interactions, improving solubility, and forcing the polymer into a glassy state with high excess free pore volume.[26]

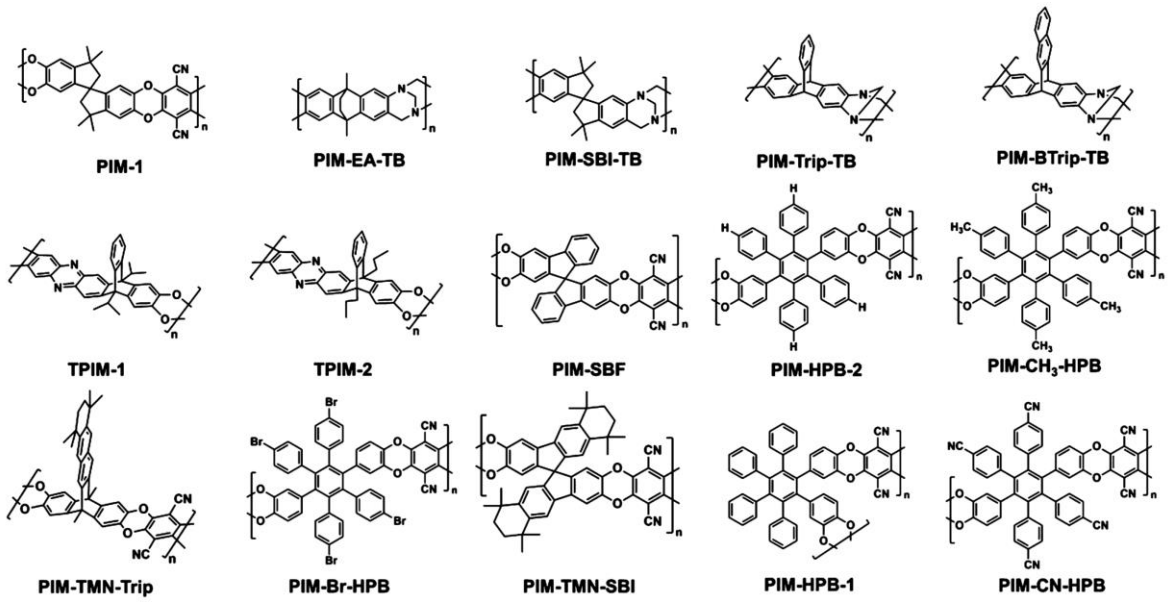

Figure 3. Typical molecular structures for polymers of intrinsic microporosity that have been employed in gas permeation studies (reprinted with permission[21]).

Although applications in gas separation, storage, and permeation have been intensely studied,[27] only some of the structures shown in Figure 3 have so far been studied in contact to the liquid phase and in electrochemical applications.[9] The range of structural motifs in PIMs is rapidly expanding[28] and (post-)functionalisation strategies have been developed[29,30] to further tune the properties of these materials. New computational methods are developed to make structure-property relationships more predictable.[31]

3. Electrochemical Methods Based on PIM-Modified Electrodes and Membranes

Electrode modification by PIMs is facilitated and readily achieved by using drop-casting or spin-coating of the selectively organic-soluble polymers (e.g. chloroform for PIM-1 or PIM-EA-TB). In initial experiments,[32] it was shown that free-standing films of PIM-EA-TB are readily protonated with the accompanying uptake of (for eample) $PdCl_4^{2-}$ anions into the microporous strucutre. Also, anionic aromatic species such as indigo carmine were immobilised into the rigid PIM host film without protonation but instead aided by a co-solvent. Both the immobilised $PdCl_4^{2-}$ and indigo carmine were shown to be electrochemically active and the PIM-EA-TB electrode coating on the electrode permeable to electrolyte.

Permeability and exceptional selectivity towards solution species has been important in the development of novel separator membranes in redox flow batteries based on PIM-1. These have been shown to provide proton permeability whilst stopping vanadium cross-over.[33] In poly-sulfide redox flow systems PIMs have been shown to inhibit poly-sulfide cross-over.[34,35,36,37,38] Selective permeability to small ionic species was shown in many cases to provide excellent separator performance based on PIMs. Initial exploratory studies have addressed applications of PIMs also as self-healing films and in corrosion science.[39,40]

In addition to providing permeability towards certain smaller species, PIMs can be employed for the immobilisation of larger molecular species. PIM materials can also be employed to immobilise a water-immiscible organic phase to form an immobilised organo-gel. Liquid-liquid voltammetry was shown to be possible based on PIM-EA-TB acting as organogel and immobilising a film of organic water-immiscible phase.[41] In this study the redox active metal complex tetraphenylporphyrinato-Mn(III)Cl or MnTPP was immobilised together with the water immiscible 4-(3-phenyl-propyl)pyridine or PPP. The redox active metal complex undergoes a Mn(II) to Mn(III) redox reaction. The resulting overall redox process can be described as a combined electron transfer (electrode | organogel) and anion transfer (electrolyte | organogel) as expressed in equation 1.[42,43]

$$MnTPP(L)_2(org) + X^-(aq) \rightleftharpoons MnTPP(L)_2^+(org) + X^-(org) + e^- \qquad (1)$$

Figure 4A shows a schematic description of the process involving Mn(II/III) oxidation coupled to the transfer of an anion from the aqueous phase into the organic gel phase. Data in Figure 4B show cyclic voltammetry responses for the Mn(II/III) oxidation accompanied by sulfate transfer. Also shown are data recorded with added $NaClO_4$. A shift of the signal to lower potentials is indicative for preferred transfer of the more hydrophobic perchlorate. Figure 4C shows spectro-electrochemical data with the Soret band shifting to longer wave length upon oxidation. The role of the PIM-EA-TB in these experiments is that of a scaffold to define the organic gel phase and the interaction with the substrate electrode. Note the

mechanistic complexity due to coupled electron and ion transport in the rigid PIM environment.

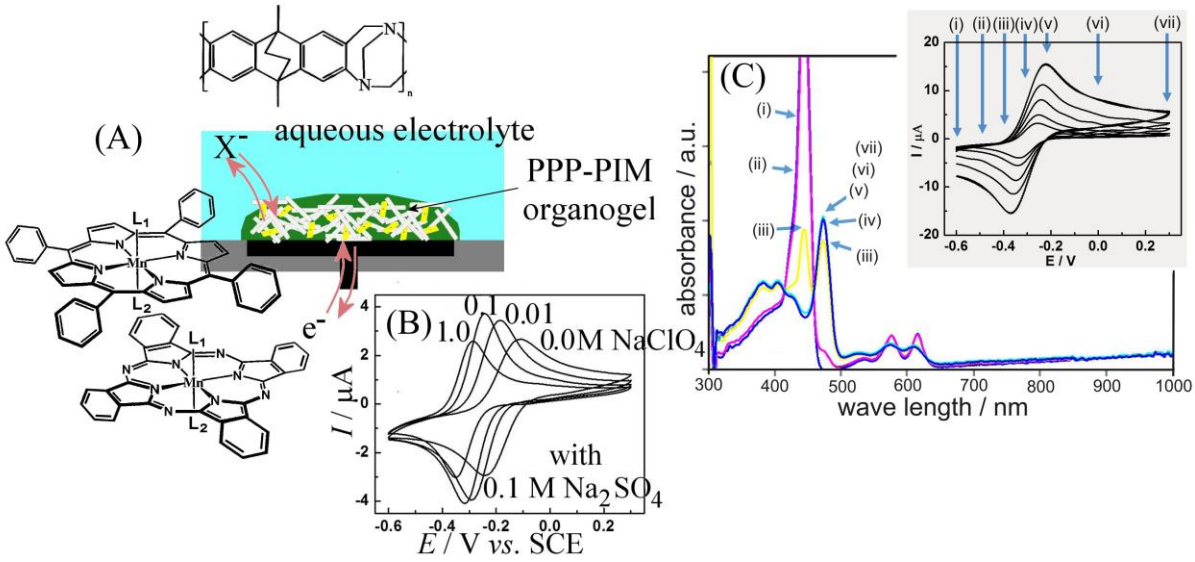

Figure 4. (A) Molecular structures of PIM-EA-TB and the metal complexes MnTPP and MnPc. (B) Cyclic voltammograms (scan rate 10 mV s^{-1}) for a deposit of MnTPP-PIM-EA-TB in 4-(3-phenyl)-propylpyridine organogel on a 3 mm diameter glassy carbon electrode immersed into aqueous 0.1 M Na_2SO_4 with 0.0, 0.01, 0.1, or 1.0 M $NaClO_4$. (C) Spectroelectrochemical data for MnTPP-PIM-EA-TB-PPP organogel immobilized onto porous ITO and immersed into aqueous 0.1 M $NaClO_4$ with applied potential indicated (reprinted with permission[41]).

In order to dissect ion transport from other aspects of the mechanism, PIM-EA-TB has been studied as free-standing membrane when immobilised onto a poly-ethylene-terephthalate film with a microhole.[44] Figure 5B and 5C show the electrochemical cell configuration and the microhole substrate. When immersed in aqueous 10 mM NaCl on both sides, pH-dependent conductivity is observed with impedance spectroscopy (see Figure 5D) consistent with a pK_A of the tertiary amine of approximately 4. Ionic conductivity in neutral solution is associated with both cation and anion transport. However, at more acidic pH < 4 anion transport dominates and semi-permeable behaviour is observed. This is manifest in ionic rectifier or diode behaviour,[45] but also shown to lead to additional ionic diode switching in the presence of a multi-basic acid such as phytic acid (Figure 5E,F). The ionic diode phenomenon has been suggested to be applicable in an AC-driven desalination system.[46]

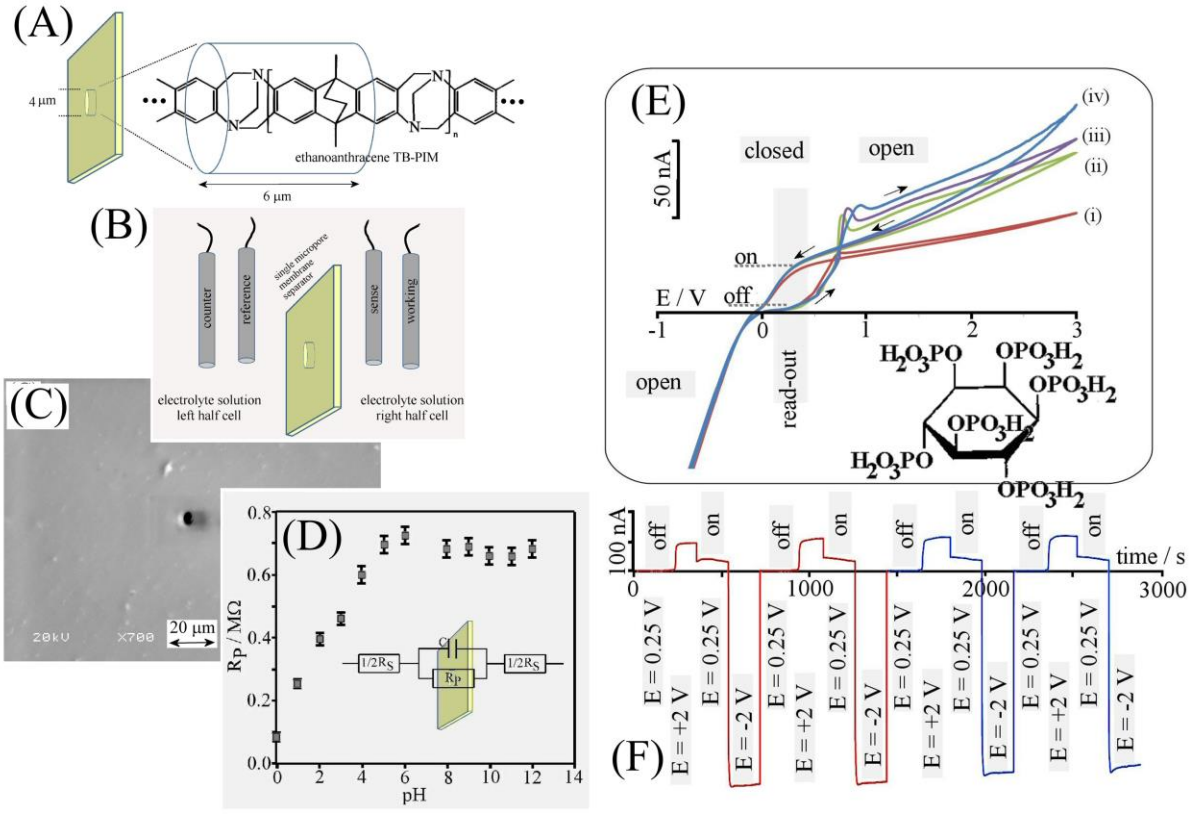

Figure 5. Schematic drawing of (A) the molecular structure of PIM-EA-TB and (B) the electrochemical cell with left and right half cells filled with electrolyte. (C) Scanning electron micrograph of the PET membrane (6 µm thickness) with a single hole (ca. 4 µm diameter) laser machined into the centre. (D) Equivalent circuit employed for impedance data analysis (at 0.0 V vs. SCE) and plot of R_P (fitting error below 1%; error bars estimated) at open circuit potential *versus* pH. (E) Experimental voltammograms (four consecutive cycles, scan rate 0.02 Vs^{-1}) in 10 mM HCl (left) – 10 mM NaOH (right) with 1 mM phytate added. Hysteresis and bistable switching occurs at 0.25 V vs. SCE. The molecular structure of phytic acid is shown. (F) Chronoamperometry for potential step switching and on/off behaviour as a function of time (Reprinted with permission[44]).

A pH-switchable ionic diode response was observed with a very thin 200 nm PIM-EA-TB film spin coated and then lifted to transfer to the poly-ethylene-terephthalate microhole substrate.[47] A link of competing anion and cation transport rates to partial semi-conductivity and diode effects in PIM-EA-TB has been proposed.[48] Also, a "hetero-junction" diode based on PIM-EA-TB in contact to Nafion has been proposed to function as a sensor diode sensitive to perchlorate and potassium cations.[49,50] Electroluminescence phenomena were observed (but not fully explained) with the highly fluorescence PIM-1 deposited onto tin-doped indium oxide electrodes.[51]

4. Electrochemical Processes within PIM Membranes

It is easily conceivable to employ the PIM film immobilised on an electrode surface as a rigid environment for immobilisation of molecular or nanoparticulate catalysts. The microporous environment created by the PIM can be employed to create a scaffold system for water-insoluble catalysts to be dispersed, and to allow reagents and buffer from bulk solution to reach the immobilised catalyst in a 3-dimensional microporous structure. Furthermore, the PIM film can provide size selectivity and effects due to partitioning of hydrophobic reagents during the catalytic reaction.

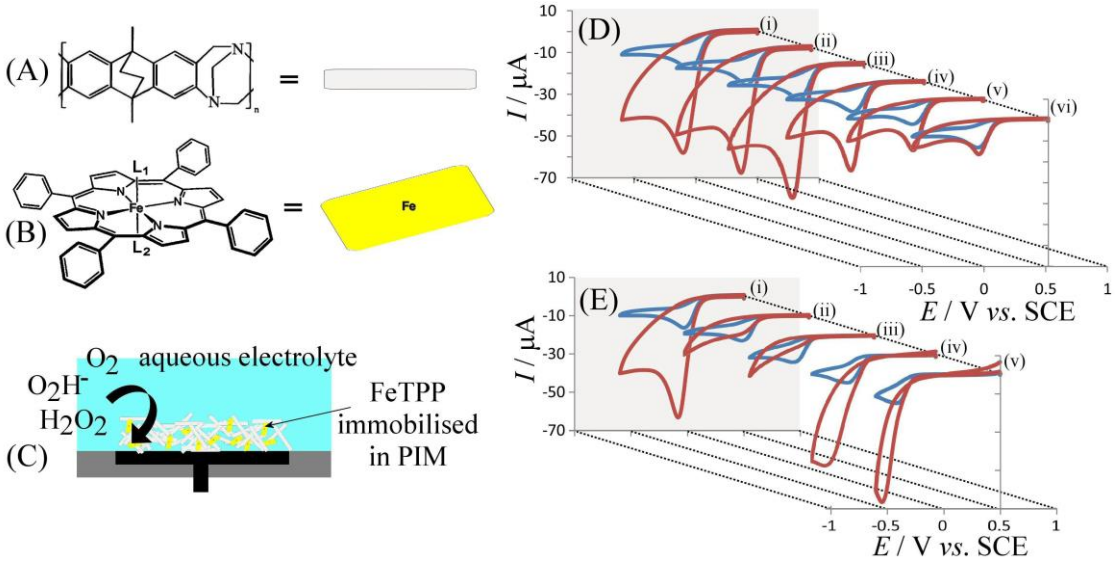

Figure 6. (A) Molecular structure of PIM-EA-TB and (B) of FeTPP. Schematic drawings of (C) FeTPP immobilised into the rigid microporous structure. (D) Cyclic voltammograms (scan rate 20 mVs^{-1}) for the reduction of ambient oxygen (blue) and 4 mM H_2O_2 (red) at electrodes coated with (i) 1:1, (ii) 1:2, (iii) 1:5, (iv) 1:10, (v) 1:20, and (vi) 1:40 weight ratio FeTPP:PIM immersed in aqueous 0.1 M phosphate buffer pH 2. (E) Cyclic voltammograms (scan rate 20 mVs^{-1}) for the reduction of ambient oxygen (blue) and 4 mM H_2O_2 (red) at electrodes coated with 1:5 FeTPP:PIM immersed in aqueous 0.1 M phosphate buffer at pH (i) 2, (ii) 4, (iii) 7, (iv) 9, and (v) 12 (reprinted with permission[52]).

The immobilisation of tetraphenylporphyrinato-Fe(II) (FeTPP) into a film of PIM-EA-TB was reported by Rong and coworkers.[52] The PIM-EA-TB polymer was mixed in chloroform with the FeTPP metal complex and deposited together by drop casting onto a glassy carbon electrode. The presence of the FeTPP resulted in catalysis for both oxygen evolution and H_2O_2 reduction (Figure 6). When investigating the weight ratio of FeTPP to PIM-EA-TB in

the deposition solution a significant change is observed in the voltammetric response for H_2O_2 reduction at 1:5. At a ratio 1:40 the response for H_2O_2 seems very low compared to the underlying O_2 reduction. Although no full study of the mechanism was reported, it seems likely that charge carrier transport in the microporous catalyst structure is a crucial part and therefore a high density of FeTPP is more effective. When studying the effect of pH (Figure 6E) significant catalysis is observed in acidic and in alkaline conditions.

The immobilisation of 4-benzoyloxy-TEMPO into PIM-EA-TB has been reported by Ahn and coworkers.[53,54] The bulky benzoyloxy group renders the 4B-TEMPO catalyst water insoluble and easy to co-deposit from chloroform solution together with the host PIM-EA-TB. Figure 7 shows a typical SEM showing carbon microparticles coated with approximately 200 nm polymer-catalyst film. The oxidation of the 4B-TEMPO derivative was observed at pH 10.3 and used to drive the catalytic oxidation of aliphatic/aromatic alcohols. Figure 7C shows cyclic voltammetry data for the oxidation of 4B-TEMPO in the presence of (i) 4 mM ethanol, (ii) 4 mM glucose, (iii) 4 mM 3-pyridine-methanol, (iv) 4 mM benzyl alcohol. The increase in the catalytic activity in this sequence is only in part due to the intrinsic electronic reaction rate (which is dominated by hydrogen abstraction step). A strong contribution was observed from the PIM-EA-TB host material “selecting” the more hydrophobic alcohols. Therefore, a combination of kinetic selectivity, size selectivity, and hydrophobic partitioning selectivity is possible under these conditions in a PIM environment.

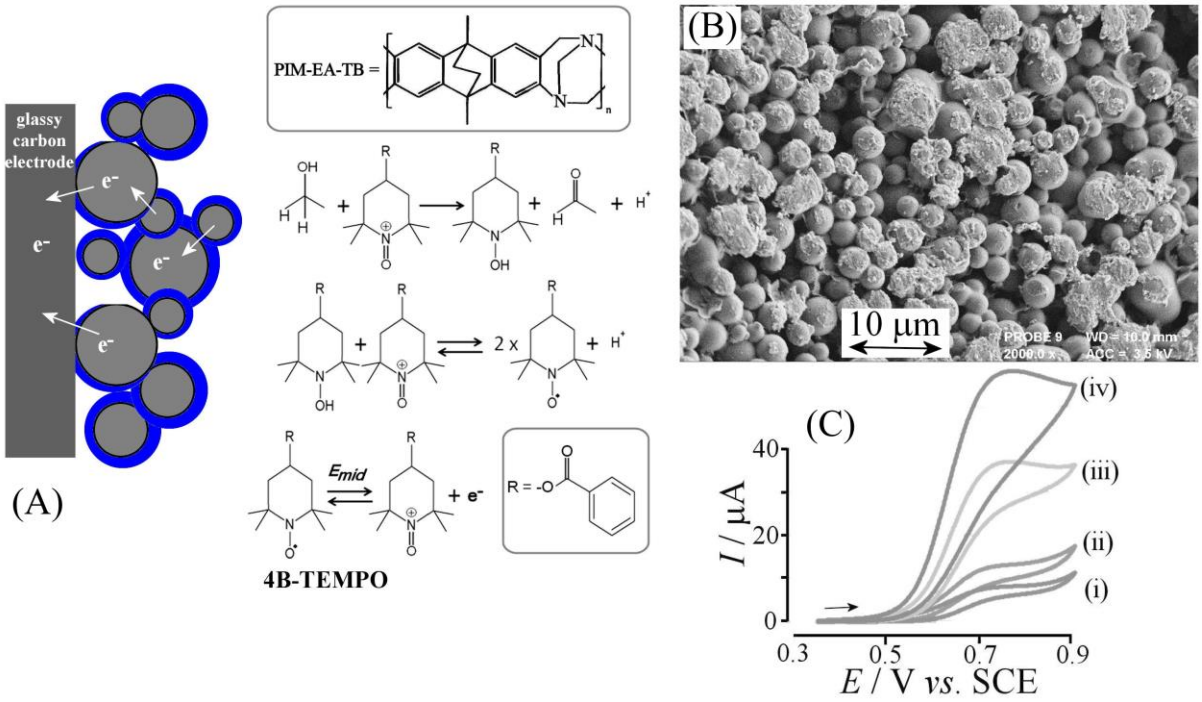

Figure 7. (A) Scheme showing the PIM-EA-TB molecular structure, 4B-TEMPO structure and reactivity, and a cartoon of the composite film with electrocatalyst embedded in PIM-EA-TB coated onto carbon microspheres. (B) SEM image for the composite film made of 0.75 μg 4B-TEMPO immobilised in 7.5 μg PIM-AT-TB with 180 μg carbon microparticles giving a porous film of approximately 50 μm thickness on a 3 mm diameter glassy carbon electrode. The thickness of the PIM-EA-TB layer around each carbon microparticle is estimated to be 50 nm. (C) Cyclic voltammograms (scan rate 10 mVs^{-1}; in 0.1 M carbonate buffer pH 10.3) with 0.75 μg 4B-TEMPO + 7.5 μg PIM-EA-TB + 180 μg carbon microparticles on a 3 mm diameter glassy carbon electrode in the presence of (i) 4 mM ethanol, (ii) 4 mM glucose, (iii) 4 mM 3-pyridine-methanol, (iv) 4 mM benzyl alcohol (reprinted with permission[53]).

5. Electrocatalytic Processes Enhanced by PIM Membranes

Nanoparticulate electrocatalyst are readily coated with PIM films. Initial work by He and coworkers with platinum nanoparticles[55] suggested that (i) the nanoparticle catalyst remains active without any blocking of the active catalyst surface (a result caused by the molecularly rigid structure of the PIM unable to block the surface), (ii) the nanoparticle catalyst is protected against corrosion phenomena involving disloged particles and surface blocking, and (iii) the nanoparticle catalyst remain active towards many types of substrates.[56] The platinum nanoparticles could aslo be stabilised/capped by PIM-EA-TB is acidic solution to

give entirely new types of composites with electrical conductivity depending on the weight ratio of Pt to PIM-EA-TB.[57]

Rong and coworkers[58] reported electrodeposited gold nanoparticles on ITO electrode substrates (see Figure 8A) as a catalyst for the oxidation of glucose in pH 7 phosphate buffer. When coated with PIM-EA-TB, this catalyst remained active. Catalyst blocking with BSA protein was clearly visible in the absence of PIM-EA-TB but was suppressed in the presence of PIM-EA-TB. In this case, PIM-EA-TB has to be envisaged as a size selective coating that retains the original gold catalyst activity and suppresses access of larger molecules such as proteins to the catalytic sites.

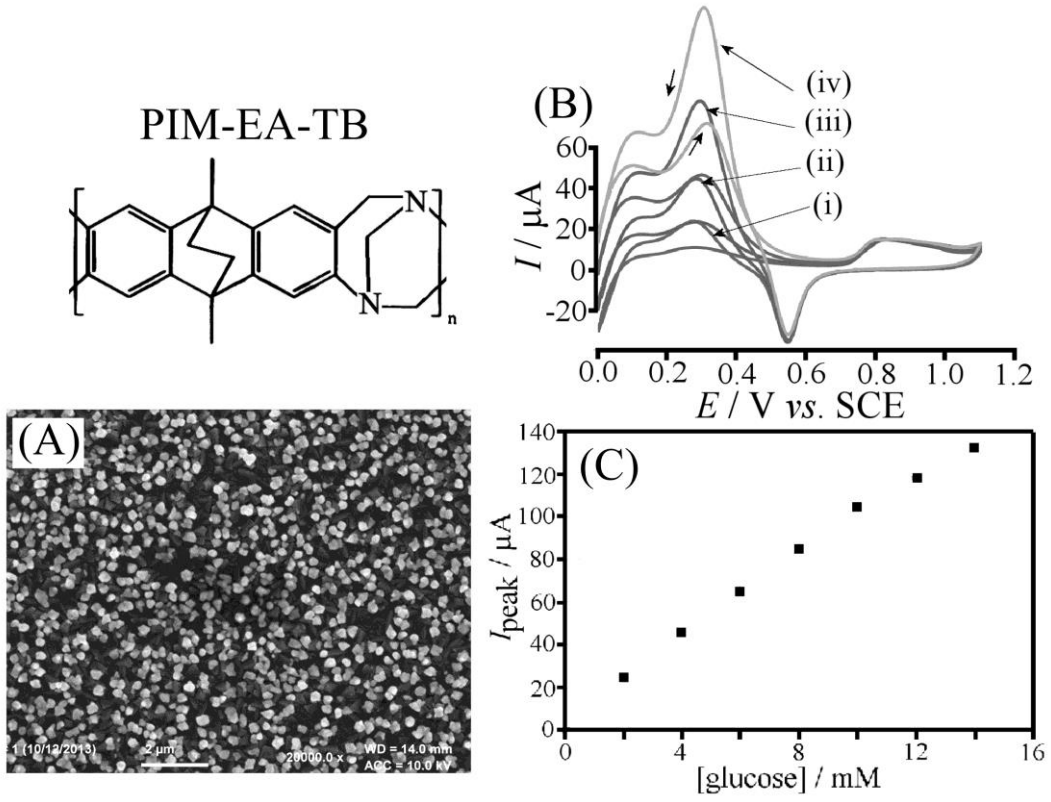

Figure 8. (A) Scanning electron microscopy images for gold nanoparticles electrodeposited onto ITO for 200 s. (B) Cyclic voltammograms (scan rate 5 mVs^{-1}, start point 0.0 V vs. SCE) for the oxidation of (i) 2, (ii) 4, (iii) 8, (iv) 14 mM glucose at gold nanoparticle on ITO, coated with 500 nm thick PIM-EA-TB film and immersed in 0.1 M phosphate buffer pH 7. (C) Plot of the peak current for glucose oxidation versus glucose concentration (reprinted with permission[58]).

Silver microparticles were immobilised onto glassy carbon and coated with PIM-EA-TB[59] to give more complex reactivity dominated by vibration sensitive nucleation phenomena at the silver | electrode interface. It is interesting to contrast the reactivity in PIM-encapsulated nanoparticle catalysts with that of carbonised PIM-encapsulated materials. For PIM-1 carbonisation resulted in a high surface area carbon material suitable for supercapacitor applications.[60] It was shown that the careful carbonisation of PIM-EA-TB produces a heterocarbon without loss of morphology or of cumulative pore volume.[61,62] The black product clearly exhibited Raman signatures for graphitic carbon, but the molecularly rigid backbone of the PIM (which is known to lead to high temperature tolerance or cross-linking for PIMs[63]) must have remained intact with also nitrogen being retained (at least at lower carbonization temperatures). Also PIM-1 was reported to carbonise to novel microporous water filtration membranes.[64] Based on these results, it seemed possible to first load PIM-EA-TB with a catalytic metal, e.g. with $PtCl_6^{2-}$ [65] or with $PdCl_4^{2-}$,[66] and then produce composite nano-catalysts in a single carbonisation process (under vacuum). Figure 9A and 9B show palladium nanoparticles (TEM and diffraction pattern) produced under these conditions embedded in carbonised PIM-EA-TB.

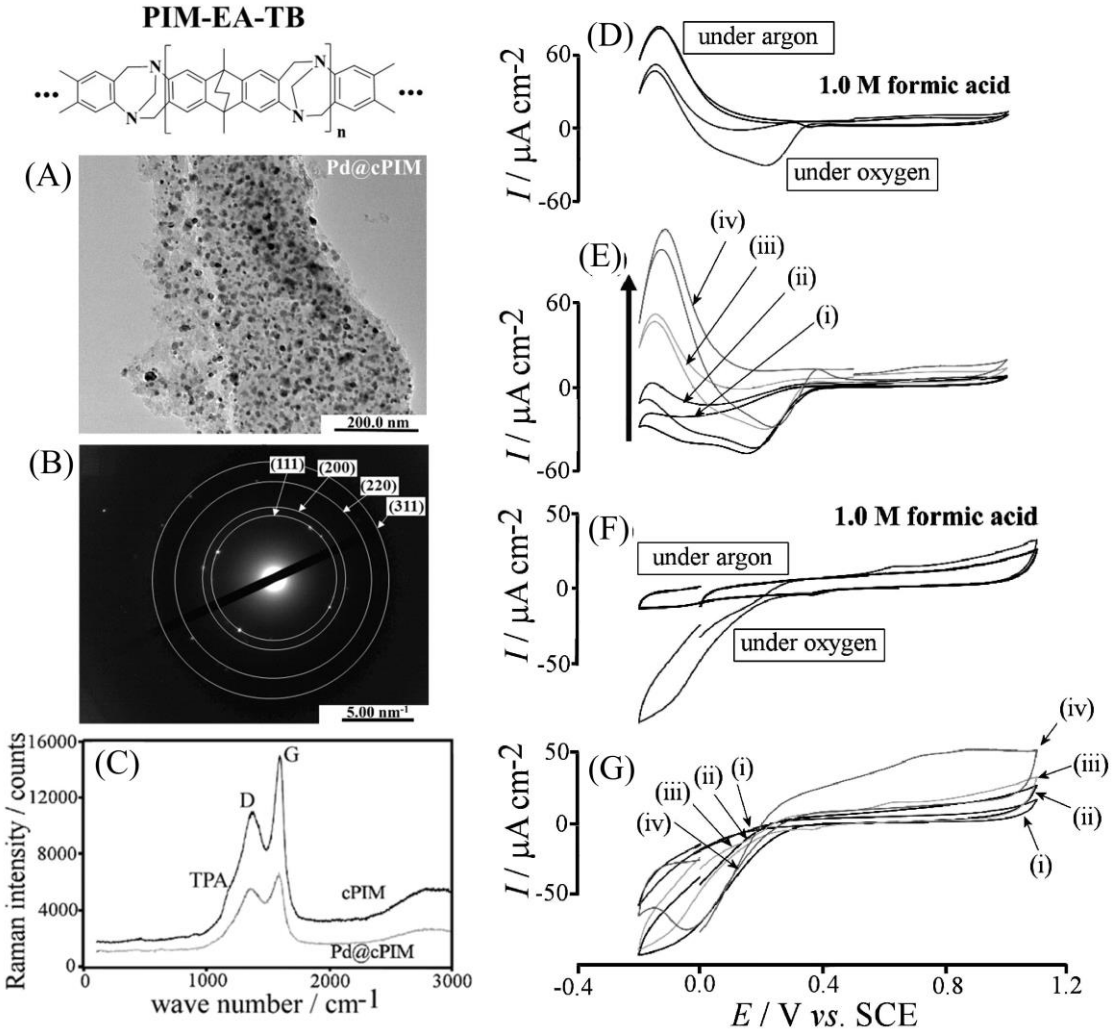

Figure 9. (A) TEM image for Pd@cPIM flakes. (B) TEM diffraction pattern for embedded nano-palladium. (C) Raman data for cPIM and Pd@cPIM showing characteristic TPA shoulder and D- and G-bands for carbon. (D,F) Cyclic voltammograms (scan rate 1 mV s^{-1}) for a bare Pd and a Pd@cPIM-modified glassy carbon in 1.0 M HCOOH under argon or oxygen saturated conditions. (E,G) Cyclic voltammograms (scan rate 1 mV s^{-1}) for a pure Pd and a Pd@cPIM-modified GC in oxygen-saturated HCOOH of varying concentrations at (i) 0.1 M, (ii) 0.5 M, (iii), 1.0 M and (iv) 5.0 M (reprinted with permission[66]).

Palladium is known to spontaneously produce hydrogen gas upon contact to formic acid[67] and this is reflected in cyclic voltammetry data. Figure 9D shows reactivity in the presence/absence of ambient oxygen with a typical hydrogen production peak (anodic) in the negative potential range. The effect of formic acid concentration is shown in Figure 9E. Perhaps surprisingly, for Pd@cPIM catalyst the spontaneous hydrogen production is not observed (Figure 9F) and instead the oxygen reduction response dominates. This is consistent with formic acid not being able to penetrate into the microporous heterocarbon. Some remaining reactivity can be seen as anodic currents in the presence of 5 M formic acid

(Figure 9G). This type of electrode in combination with bare palladium was shown to spontaneously produce energy in a single compartment cuel cell configuration.

This selectivity effect of the micropores was further utilised for a Pt@cPIM catalyst prepared from a PIM-EA-TB-H_2 precursor polymer.[68] It was demonstrated that a mixture of oxygen gas and hydrogen gas allows direct synthesis of hydrogen peroxide. The smaller hydrogen molecules were proposed to enter the composite catalyst micropores to give electrons (in the carbon structure) and protons. Oxygen is then reduced at the outer carbon shell to give hydrogen peroxide.

The selectivity for small gaseous species was observed not only for carbonised PIM materials, but also for some materials such as PIM-1.[69] PIM-1 immobilised (in nanoparticulate form) onto a platinum disk electrode and immersed into 10 mM phosphate buffer at pH 7 (see Figure 10A) caused the reduction peak for hydrogen formation to be suppressed, but new anodic peaks for hydrogen oxidation to emerge. These new peaks were explained in terms of molecular hydrogen being bound and stored in PIM-1 directly at the electrode surface. Similar results were also obtained with a film of PIM-1 (which is more sensitive towards delamination during hydrogen evolution). With initial evidence for hydrogen storage at the electrode surface, other types of electrodes and gaseous species were investigated. Most striking are the results for the reduction of oxygen at a glassy carbon electrode. The cathodic peak in voltammograms for oxygen reduction is shifted positive by approximately 150 mV indicative of a higher activity of oxygen in the presence of PIM-1 nanoparticles. Figure 10D shows data for rotating ring disc voltammetry data (for a carbon disk with variable potential to show oxygen reduction and a platinum ring with fixed potential to verify production of hydrogen peroxide).

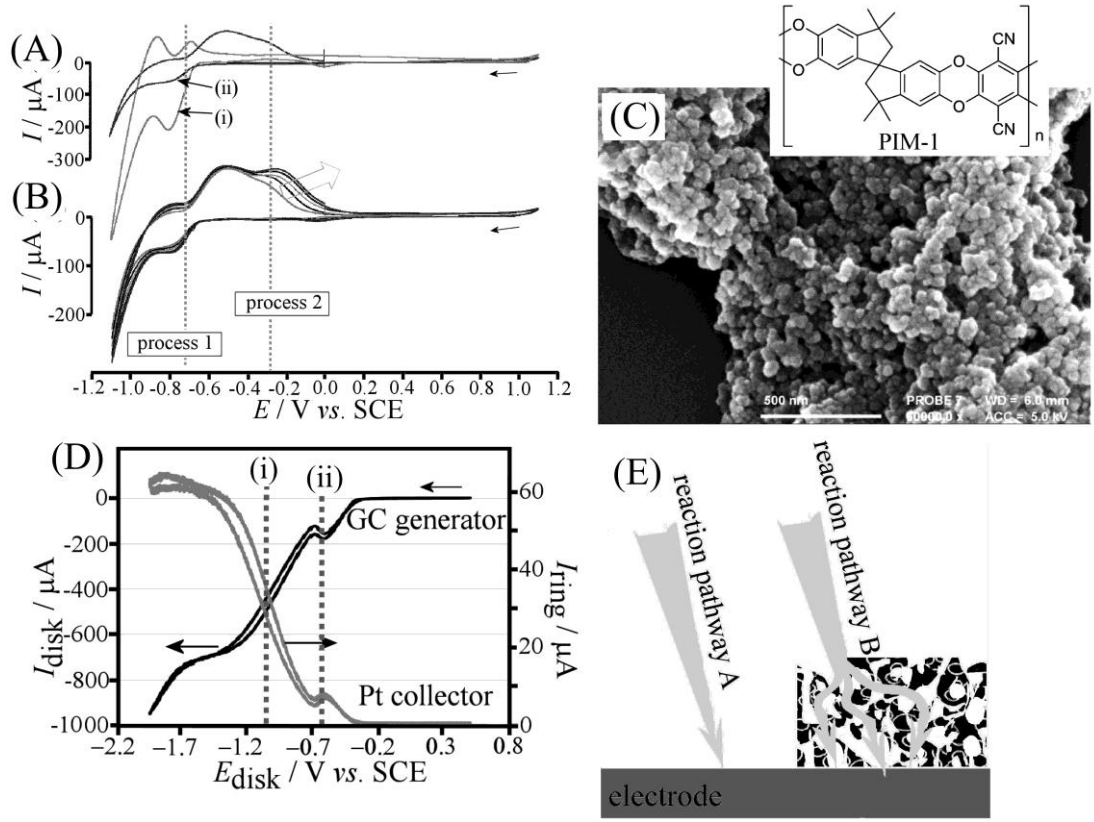

Figure 10. (A) Cyclic voltammograms (scan rate 50 mVs^{-1}) for a 3 mm diameter Pt disk electrode immersed in 0.01 M phosphate buffer pH 7.7 for (i) the bare electrode and (ii) a 20 μg PIM-1 nanoparticle deposit. (B) As before but for five consecutive potential cycles. (C) Scanning electron microscopy (SEM) images for PIM-1 nanoparticles deposited onto a carbon surface. (D) Cyclic voltammograms (scan rate 50 mVs^{-1}; rotating ring-disk electrode with a 5.5 mm diameter glassy carbon disc and a 2 mm wide platinum ring; 1500 rpm; ring potential +0.3 V vs. SCE) for the reduction of oxygen (1 bar oxygen purged solution) in 0.01 M phosphate buffer solution at pH 7 for PIM-1 nanoparticle modified glassy carbon. (E) Schematic drawing of reaction pathway A (gas molecules diffuse from solution to the electrode surface) and reaction pathway B (gas molecules accumulate in the intrinsically microporous polymer host and react at the electrode surface with apparently higher activity) (reprinted with permission[69]).

The reduction of oxygen on the carbon disk is shifted positive in the presence of PIM-1 nanoparticles and visible as a peak during forward and backward potential scans. The peaks are visible in the ring current and therefore associated with the formation of the same product, hydrogen peroxide. Two types of polymers, PIM-1 and PIM-PY, were shown to give similar results. The proposed mechanism is based on oxygen binding into the PIM-1 to form a triphasic system with an apparently higher activity of oxygen at the electrode surface.

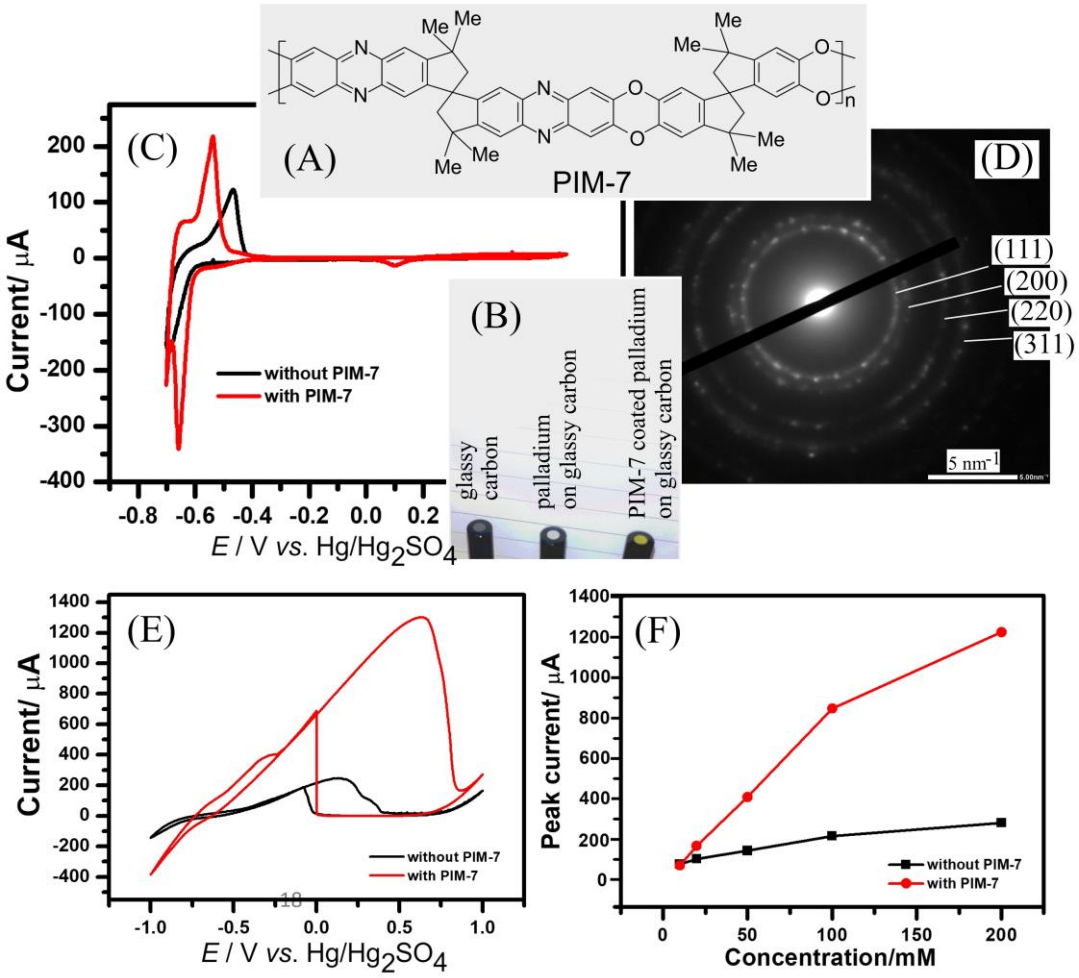

Figure 11. Polymeric structures of PIM-7. (B) Photographic image of glassy carbon, palladium on glassy carbon, and PIM-7 coated palladium on glassy carbon. (C) Cyclic voltammograms (in argon-purged solution; scan rate 20 mVs^{-1}) for a palladium-coated glassy carbon electrode (black) and for a palladium and PIM-7 coated glassy carbon electrode (red) immersed in aqueous 1 M H_2SO_4 solution over a potential window 0.7 to –0.7 V vs. Hg/Hg_2SO_4. (D) Electron diffraction data (for the central region in image B) showing the characteristic diffraction lines for palladium. (E) Cyclic voltammograms (scan rate of 100 mVs^{-1}) for a palladium-coated glassy carbon electrode (black) and for a palladium and PIM-7 coated glassy carbon electrode (red) immersed in aqueous 0.2 M formic acid solution. (F) Plot of peak currents *versus* concentration of formic acid (reprinted with permission[70]).

Further evidence for the effects of tripahisc conditions on electrodechemical processes in the presence of a PIM were repoted by Mahajan *et al.*[70] PIM-7 (see molecular structure in Figure 11) was applied to electro-deposited palladium nanoparticles on glassy carbon. Only electrode processes involving hydrogen gas were substantially affected. Figure 11C shows

data for cyclic voltammetry in 1 M H_2SO_4 with clear hydrogen intercalation peaks before hydrogen evolution at more negative applied potentials. The reversibility for the hydrogen intercalation and deintercalation (separation of voltammetric peaks) was enhanced in the presence of PIM-7. Even more dramatic was the change in the voltammetric responses for the oxidation of formic acid (Figure 11E and 11F). In particular for higher formic acid concentrations the PIM-7 film substantially increases currents and improves reversibility. In part, this can be attributed to a catalyst surface free of bubbles, but the ability of PIM-7 to capture and bind hydrogen in hydrophobic pockets may also contribute to the improved triphasic reaction conditions.

6. Photo-Electrocatalytic Processes Enhanced by PIM Membranes

Among the very important photo-electrochemical processes in the development of sustainable energy technology[71] is the production of hydrogen gas driven by sunlight, for example at semiconductors.[72] This is commonly achieved with a photo-active semiconductor material able to absorb the light and to generate (an exciton followed by) short-lived species termed holes (in the valence band) and electrons (in the conduction band). These "charge carriers" need to be separated and transferred to an external electrode surface. The associated need for electrical conductivity is often linked to high temperature processing of electrodes to overcome resistance in grain boundaries. Here, the alternative strategy of an "energy carrier" based on hydrogen gas transported in a PIM film is discussed as an alternative to charge carrier transport.[73]

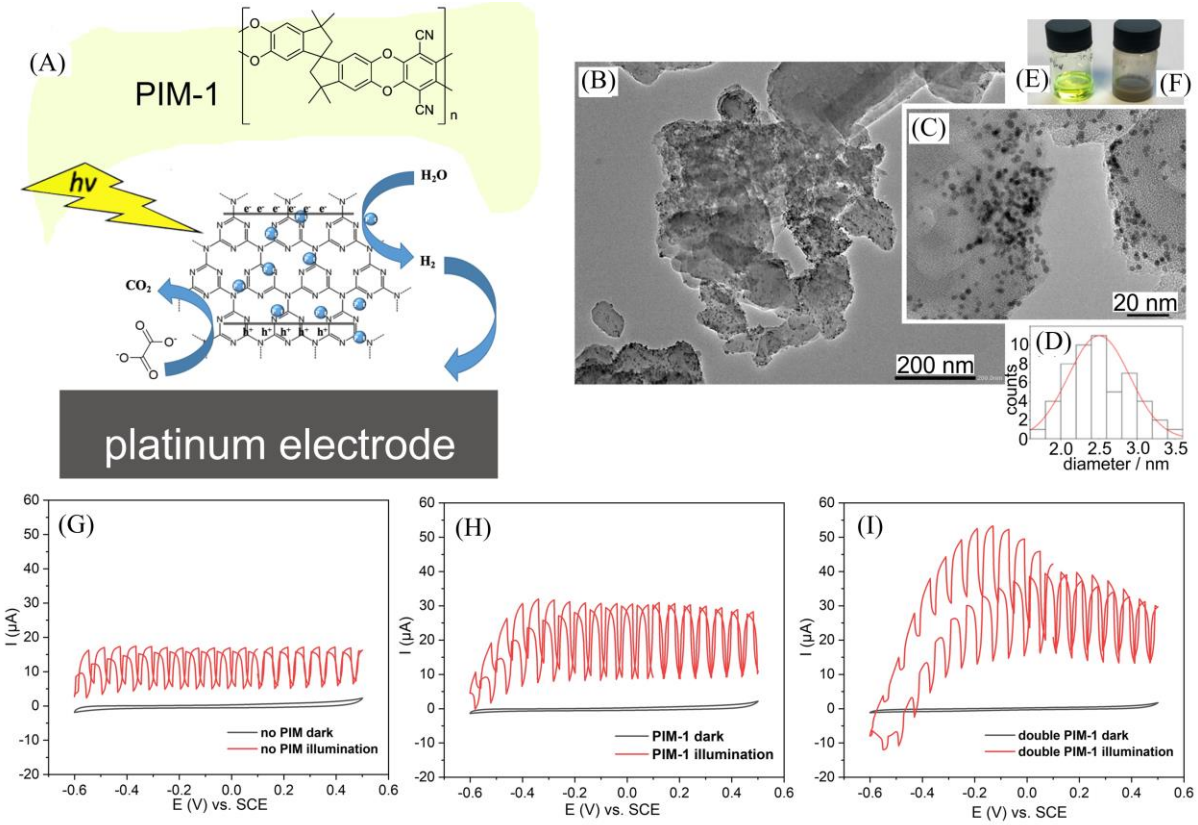

Figure 12. (A) Schematic illustration of Pt@g-C_3N_4 photocatalyst at a platinum electrode surface generating hydrogen. A PIM-1 coating is applied to provide mechanical stability, to capture hydrogen, and to provide triphasic reaction conditions. (B,C) Characterisation of Pt@g-C_3N_4 with TEM. (D) Histogram of the platinum nanoparticle size distribution with maximum at diameter 2.5 nm. (E) Photographic image of PIM-1 solution in chloroform and (F) of the Pt@g-C_3N_4 suspension in isopropanol. (G-I) Cyclic voltammograms (scan rate 20 mVs^{-1}; black = no illumination; red = 2 s on and 1 s off, 385 nm LED) at a 3 mm diameter platinum disk electrode coated with Pt@g-C_3N_4 and immersed in 0.3 M disodium oxalate; (G) under argon with 75 μg Pt@g-C_3N_4; (H) as before with 10 μg PIM-1; (I) as before with 20 μg PIM-1 (reprinted with permission[73]).

Figure 12A shows schematically the concept of the photo-catalyst Pt@g-C_3N_4 immobilised at the surface of a platinum electrode. Light pulses in the presence of a sacrificial hole quencher lead to the production of hydrogen close to the electrode surface. A film of PIM-1 coated over the assembly not only provides additional mechanical robustness, but also helps capturing the evolving hydrogen. In Figure 12G-I, the effect of the PIM-1 on the photocurrent is demonstrated. The increase in the photo-current response with the thicker PIM-1 deposit is associated with a shift of the photocurrent onset to more positive potentials. This is linked to the build up of proton concentration close to the electrode surface under the PIM-1 coating. The overall mechanism can be written as excitation (2), charge separation (3), hole quenching

(4), hydrogen evolution (5), and transport of molecular hydrogen to the electrode for discharge (6).

$$Pt@g\text{-}C_3N_4 + h\nu \longrightarrow Pt@g\text{-}C_3N_4^* \quad (2)$$

$$Pt@g\text{-}C_3N_4^* \longrightarrow Pt^-@g\text{-}C_3N_4^+ \quad (3)$$

$$Pt^-@g\text{-}C_3N_4^+ + \tfrac{1}{2}\ oxalate^{2-} \longrightarrow Pt^-@g\text{-}C_3N_4 + CO_2 \quad (4)$$

$$Pt^-@g\text{-}C_3N_4 + H^+ \longrightarrow \tfrac{1}{2}\ H_2 \quad (5)$$

$$H_2 \longrightarrow 2\ H^+ + 2\ e^-(platinum) \quad (6)$$

The oxalate is employed here as a sacrificial hole quencher and other types of quenchers have been demonstrated including glucose (as a model for biomass).[67] Components used in this assembly are fully room temperature printable (without the need for high temperature processing that is required for semiconductor components with charge carrier transport). In the future, with further improvements in the molecular structure of the PIM and the device architecture, the photo-current and energy harvesting efficiency can be further increased.

7. Conclusion and Outlook

The effects of polymers of intrinsic microporosity (PIMs) on some electrochemical processes has been assessed. Important progress is reported in particular for PIMs as selective membranes, but also in the observation of multi-phase processes that are enhanced by PIMs coated as a film or nanoparticulate film directly over the electrode surface. Nanoparticulate and molecular catalysts were immobilised into the rigid molecular environment in the vicinity of the electrode. Also, water immiscible liquid phase immobilisation has been demonstrated to lead to electrochemically driven liquid-liquid ion exchange. There is considerable complexity in terms of mechanism and in terms of coupled ion/electron transport in many of these systems and experimental work so far is mostly exploratory in nature.

The effects of PIM coatings on gas evolving and gas consuming electrochemical reactions was noted for materials such as PIM-1, PIM-7, and PIM-PY (but not observed for PIM-EA-

TB) and there are probably other types of microporous polymers with similar or improved behaviour. For hydrogen evolving processes, a gas capture effect was noted as well as an enhanced reactivity of the catalytic surface, which has been assigned to avoided bubble nucleation/blocking and increase solute activity or supersaturation close to the electrode surface. More work will be required to better resolve both the chemical and the physical reasons and for implications/applications of these effects, for example in the field of gas diffusion electrodes. There are considerable technical and theory challenges in order to provide a better fundamental in depth understanding of multi-phase processes in microporous environments. Some of these may be addressed only by a combination of modern *in operando* spectro- or diffracto-electrochemical tools in conjunction with computer simulation.

It is obvious that there are many potential types of PIMs with many diverse types of molecular structures. Work at this stage is mainly exploratory in nature and further insight into processes and mechanisms at molecular level will be desirable. In particular computational tools could be important in future to further develop molecular level understanding and to predict new improved molecular structures for PIMs to enhance reactivity in triphasic (electro-)catalysis.

Acknowledgements

E.M. thanks the EPSRC (EP/K004956/1). E.M. and N.B.M. thank the Leverhulme Foundation (RPG-2014-308: "New Materials for Ionic Diodes and Ionic Photodiodes") for financial support. Y.Z. thanks the China Scholarship Council (CSC scholarship No 20180935006) for a PhD scholarship.

References

[1] F.L. Lyu, Q.F. Wang, S.M. Choi, Y.D. Yin, Small 2019, 15, 1804201.

[2] J.F. Xie, Y.Y. Huang, M.X. Wu, Y.B. Wang, *ChemElectroChem* **2019**, *6*, 1587–1604.

[3] C.E. Banks, T.J. Davies, R.G. Evans, G. Hignett, A.J. Wain, N.S. Lawrence, J.D. Wadhawan, F. Marken, R.G. Compton, *Phys. Chem. Chem. Phys.* **2003**, *5*, 4053–4069.

[4] F. Marken, J.D. Watkins, A.M. Collins, *Phys. Chem. Chem. Phys.* **2011**, *13*, 10036–10047.

[5] A.M. Soto, S.R. German, H. Ren, D. van der Meer, D. Lohse, M.A. Edwards, H.S. White, *Langmuir* **2018**, *34*, 7309–7318.

[6] U. Hasse, S. Fletcher, F. Scholz, *J. Solid State Electrochem.* **2006**, *10*, 833–840.

[7] K.J. Stevenson, K. Tschulik, *Curr. Opinion Electrochem.* **2017**, *6*, 38–45.

[8] J. Li, G.X. Chen, Y.Y. Zhu, Z. Liang, A. Pei, C.L. Wu, H.X. Wang, H.R. Lee, K. Liu, S. Chu, Y. Cui, *Nature Catal.* **2018**, *1*, 592–600.

[9] J. Li, Y.Y. Zhu, W. Chen, Z.Y. Lu, J.W. Xu, A. Pei, Y.C. Peng, X.L. Zheng, Z.W. Zhang, S. Chu, Y. Cui, *Joule* **2019**, *3*, 557–569.

[10] J.B. Vennekoetter, R. Sengpiel, M. Wessling, *Chem. Engineer. J.* **2019**, *364*, 89–101.

[11] M.Y. Wang, X.T. Yu, Z. Wang, X.Z. Gong, Z.C. Guo, L. Dai, *J. Mater. Chem. A* **2017**, *5*, 9488–9513.

[12] S.R. German, M.A. Edwards, H. Ren, H.S. White, *J. Amer. Chem. Soc.* **2018**, *140*, 4047–4053.

[13] E. Madrid, N.B. McKeown, *Curr. Opinion Electrochem.* **2018**, *10*, 61–66.

[14] S. Witharana, B. Phillips, S. Strobel, H.D. Kim, T. McKrell, J.B. Chang, J. Buongiorno, K.K. Berggren, L. Chen, Y. Ding, *J. Appl. Phys.* **2012**, *112*, 064904.

[15] S.D. Lubetkin, *Langmuir* **2003**, *19*, 2575–2587.

[16] N. Masoumifard, R. Guillet-Nicolas, F. Kleitz, *Adv. Mater.* **2018**, *30*, 1704439.

[17] A. Feliczak-Guzik, *Micropor. Mesopor. Mater.* **2018**, *259*, 33–45.

[18] Y.Q. Xue, S.S. Zheng, H.G. Xue, H. Pang, *J. Mater. Chem. A* **2019**, *7*, 7301–7327.

[19] H. Barike Aiyappa, J. Masa, C. Andronescu, M. Muhler, R.A. Fischer, W. Schuhmann, *Small Methods* **2018**, 1800415.

[20] S.M.J. Rogge, A. Bavykina, J. Hajek, H. Garcia, A.I. Olivos-Suarez, A. Sepulveda-Escribano, A. Vimont, G. Clet, P. Bazin, F. Kapteijn, M. Daturi, E.V. Ramos-Fernandez, F.X.L.I. Xamena, V. Van Speybroeck, J. Gascon, *Chem. Soc. Rev.* **2017**, *46*, 3134–3184.

[21] Z.X. Low, P.M. Budd, N.B. McKeown, D.A. Patterson, *Chem. Rev.* **2018**, *118*, 5871–5911.

[22] C. Ma, J.J. Urban, *Proc. Nat. Res. Soc.* **2018,** *2*, 02002.

[23] Q. Song, S. Cao, R.H. Pritchard, B. Ghalei, S.A. Al-Muhtaseb, E.M. Terentjev, A.K. Cheetham, E. Sivaniah, *Nature Commun.* **2014,** *5*, 4813.

[24] N.B. McKeown, *ISRN Mater. Sci.* **2012**, 513986.

[25] N.B. McKeown, P.M. Budd, *Macromolecules* **2010**, *43*, 5163–5176.

[26] N.B. McKeown, P.M. Budd, K.J. Msayib, B.S. Ghanem, H.J. Kingston, C.E. Tattershall, S. Makhseed, K.J. Reynolds, D. Fritsch, *Chem. Europ. J.* **2005**, *11*, 2610–2620.

[27] D. Ramimoghadam, E.M. Gray, C.J. Webb, *Inter. J. Hydrogen Energy* **2016,** *41*, 16944–16965.

[28] N.Y. Du, G.P. Robertson, I. Pinnau, M.D. Guiver, *Macromolecules* **2010**, *43*, 8580–8587.

[29] K. Halder, S. Neumann, G. Bengtson, M. Munir Khan, V. Filiz, V. Abetz, *Macromolecules* **2018**, *51*, 7309–7319.

[30] G. Bengtson, S. Neumann, V. Filiz, *Membranes* **2017**, *7*, 28.

[31] G.S. Larsen, P. Lin, K.E. Hart, C.M. Colina, *Macromolecules* **2011**, *44*, 6944–6951.

[32] F.J. Xia, M. Pan, S.C. Mu, R. Malpass-Evans, M. Carta, N.B. McKeown, G.A. Attard, A. Brew, D.J. Morgan, F. Marken, *Electrochim. Acta* **2014,** *128*, 3–9.

[33] I.S. Chae, T. Luo, G.H. Moon, W. Ogieglo, Y.S. Kang, M. Wessling, *Adv. Energy Mater.* **2016,** *6*, 1600517.

[34] S.E. Doris, A.L. Ward, A. Baskin, P.D. Frischmann, N. Gavvalapalli, E. Chénard, C.S. Sevov, D. Prendergast, J.S. Moore, B.A. Helms, *Angew. Chem. Inter. Ed.* **2017,** *56*, 1595–1599.

[35] S.E. Doris, A.L. Ward, P.D. Frischmann, L. Li, B.A. Helms, *J. Mater. Chem. A* **2016,** *4*, 16946–16952.

[36] C.Y. Li, A.L. Ward, S.E. Doris, T.A. Pascal, D. Prendergast, B.A. Helms, *Nano Lett*. **2015**, *15*, 5724–5729.

[37] X.W. Yu, S.N. Feng, M.J. Boyer, M. Lee, R.C. Ferrier, N.A. Lynd, G.S. Hwang, G.B. Wang, S. Swinnea, A. Manthiram, *Mater. Today Energy* **2018**, *7*, 98–104.

[38] A.L. Ward, S.E. Doris, L. Li, M.A. Hughes, X. Qu, K.A. Persson, B.A. Helms, *ACS Central Sci.* **2017,** *3*, 399–406.

[39] Z. Li, B. Qin, X. Zhang, K. Wang, Y. Wei, Y. Ji, *RSC Adv.* **2015,** *5*, 104451–104457.

[40] A.R. Langley, M. Carta, R. Malpass-Evans, N.B. McKeown, J.H.P. Dawes, E. Murphy, F. Marken, *Electrochim. Acta* **2018,** *260*, 348–357.

[41] V. Ganesan, E. Madrid, R. Malpass-Evans, M. Carta, N.B. McKeown F. Marken, *Electrocatalysis* **2018**, doi 10.1007/s12678-018-0497-8

[42] M.A. Ghanem, F. Marken, *Electrochem. Commun.* **2005**, *7*, 1333–1336.

[43] M.J. Bonné, C. Reynolds, S. Yates, G. Shul, J. Niedziolka, M. Opallo, F. Marken, *New J. Chem.* **2006**, *30*, 327–331.

[44] E. Madrid, Y.Y. Rong, M. Carta, N.B. McKeown, R. Malpass-Evans, G.A. Attard, T.J. Clarke, S.H. Taylor, Y.T. Long, F. Marken, *Angew. Chem. Internat. Ed.* **2014,** *53*, 10751–10754.

[45] K. Mathwig, B.D.B. Aaronson, F. Marken, *ChemElectroChem* **2018**, *5*, 897–901.

[46] E. Madrid, P. Cottis, Y.Y. Rong, A.T. Rogers, J.M. Stone, R. Malpass-Evans, M. Carta, N.B. McKeown, F. Marken, *J. Mater. Chem. A* **2015,** *3*, 15849–15853.

[47] Y.Y. Rong, Q. Song, K. Mathwig, E. Madrid, D. He, R.G. Niemann, P.J. Cameron, S.E.C. Dale, S. Bending, M. Carta, R. Malpass-Evans, N.B. McKeown, F. Marken, *Electrochem. Commun.* **2016,** *69*, 41–45.

[48] Y.Y. Rong, A. Kolodziej, E. Madrid, M. Carta, R. Malpass-Evans, N.B. McKeown, F. Marken, *J. Electroanal. Chem.* **2016**, *779*, 241–249.

[49] B.R. Putra, B.D.B. Aaronson, E. Madrid, K. Mathwig, M. Carta, R. Malpass-Evans, N.B. McKeown, F. Marken, *Electroanalysis* **2017**, *29*, 2217–2223.

[50] B.R. Putra, M. Carta, R. Malpass-Evans, N.B. McKeown, F. Marken, *Electrochim. Acta* **2017**, *258*, 807–813.

[51] E. Madrid, D.P. He, J.L. Yang, C.F. Hogan, B. Stringer, K.J. Msayib, N.B. McKeown, P.R. Raithby, F. Marken, *ChemElectroChem* **2016**, *3*, 2160–2164.

[52] Y.Y. Rong, R. Malpass-Evans, M. Carta, N.B. McKeown, G.A. Attard, F. Marken, *Electrochem. Commun.* **2014,** *46*, 26–29.

[53] S.D. Ahn, A. Kolodziej, R. Malpass-Evans, M. Carta, N.B. McKeown, S.D. Bull, A. Buchard, F. Marken, *Electrocatalysis* **2016**, *7*, 70–78.

[54] A. Kolodziej, S.D. Ahn, M. Carta, R. Malpass-Evans, N.B. McKeown, R.S.L. Chapman, S.D. Bull, F. Marken, *Electrochim. Acta* **2015,** *160*, 195–201.

[55] D.P. He, Y.Y. Rong, Z. Kou, S. Mu, T. Peng, R. Malpass-Evans, M. Carta, N.B. McKeown, F. Marken, *Electrochem. Commun.* **2015,** *59*, 72–76.

[56] D.P. He, Y.Y. Rong, M. Carta, R. Malpass-Evans, N.B. McKeown, F. Marken, *RSC Adv.* **2016**, *6*, 9315–9319.

[57] D.P. He, D.S. He, J.L. Yang, Z.X. Low, R. Malpass-Evans, M. Carta, N.B. McKeown, F. Marken, *ACS Appl. Mater. Interfaces* **2016**, *8*, 22425–22430.

[58] Y.Y. Rong, R. Malpass-Evans, M. Carta, N.B. McKeown, G.A. Attard, F. Marken, *Electroanalysis* **2014,** *26*, 904–909.

[59] D.P. He, E. Rauwel, R. Malpass-Evans, M. Carta, N.B. McKeown, D.B. Gorle, M.A. Kulandainathan, F. Marken, *J. Solid State Electrochem.* **2017,** *21*, 2141–2146.

[60] J.W. Jeon, J.H. Han, S.K. Kim, D.G. Kim, Y.S. Kim, D.H. Suh, Y.T. Hong, T.H. Kim, B.G. Kim, *J. Mater. Chem. A* **2018**, *6*, 8909–8915.

[61] Y.Y. Rong, D.P. He, A. Sanchez-Fernandez, C. Evans, K.J. Edler, R. Malpass-Evans, M. Carta, N.B. McKeown, T.J. Clarke, S.H. Taylor, A.J. Wain, J.M. Mitchels, F. Marken, *Langmuir* **2015,** *31*, 12300–12306.

[62] N. Hernandez, J. Iniesta, V.M. Leguey, R. Armstrong, S.H. Taylor, E. Madrid, Y.Y. Rong, R. Castaing, R. Malpass-Evans, M. Carta, N.B. McKeown, F. Marken, *Appl. Mater. Today* **2017,** *9*, 136–144.

[63] F.Y. Li, Y.C. Xiao, T.S. Chung, S. Kawi, *Macromolecules* **2012**, *45*, 1427–1437.

[64] H.J. Kim, D.G. Kim, K. Lee, Y. Baek, Y. Yoo, Y.S. Kim, B.G. Kim, J.C. Lee, *Sci. Reports* **2016**, *6*, 36078.

[65] Y.Y. Rong, D.P. He, R. Malpass-Evans, M. Carta, N.B. McKeown, M.F. Gromboni, L.H. Mascaro, G.W. Nelson, J.S. Foord, P. Holdway, S.E.C. Dale, S. Bending, F. Marken, *Electrocatalysis* **2017,** *8*, 132–143

[66] S.X. Leong, M. Carta, R. Malpass-Evans, N.B. McKeown, E. Madrid, F. Marken, *Electrochem. Commun.* **2018**, *86*, 17–20.

[67] Q.Y. Bi, J.D. Lin, Y.M. Liu, H.Y. He, F.Q. Huang, Y. Cao, *Angew. Chem. Inter. Ed.* **2016**, *55*, 11849–11853.

[68] R.K. Adamik, N. Hernandez-Ibanez, J. Iniesta, J.K. Edwards, A.G.R. Howe, R.D. Armstrong, S.H. Taylor, A. Roldan, Y.Y. Rong, R. Malpass-Evans, M. Carta, N.B. McKeown, D.P. He, F. Marken, *Nanomaterials* **2018**, *8*, 542.

[69] E. Madrid, J.P. Lowe, K.J. Msayib, N.B. McKeown, Q.L. Song, G.A. Attard, T. Düren, F. Marken, *ChemElectroChem* **2019**, *6*, 252–259.

[70] A. Mahajan, S.K. Bhattacharya, S. Rochat, A.D. Burrows, P.J. Fletcher,Y.Y. Rong, A.B. Dalton, N.B. McKeown, F. Marken, *ChemEletroChem*, **2018**, doi 10.1002/celc.201801359.

[71] S. Ardo, D.F. Rivas, M.A. Modestino, V.S. Greiving, F.F. Abdi, E.A. Llado, V. Artero, K. Ayers, C. Battaglia, J.P. Becker, D. Bederak, A. Berger, F. Buda, E. Chinello, B. Dam, V. Di Palma, T. Edvinsson, K. Fujii, H. Gardeniers, H. Geerlings, S.M.H. Hashemi, S. Haussener, F. Houle, J. Huskens, B.D. James, K. Konrad, A. Kudo, P.P. Kunturu, D. Lohse, B. Mei, E.L. Miller, G.F. Moore, J. Muller, K.L. Orchard, T.E. Rosser, F.H. Saadi, J.W. Schuttauf, B. Seger, S.W. Sheehan, W.A. Smith, J. Spurgeon, M.H. Tang, R. van de Krol, P.C.K. Vesborg, P. Westerik, *Energy Environm. Sci.* **2018**, *11*, 2768–2783.

[72] M. Ahmed, I. Dincer, Internat. J. Hydrogen Energy 2019, 44, 2474–2507.

[73] Y.Z. Zhao, N.A. Al Abass, R. Malpass-Evans, M. Carta, N.B. McKeown, E. Madrid, P.J. Fletcher, F. Marken, *Electrochem. Commun*. **2019**, doi 10.1016/j.elecom.2019.04.006.